PSFC/JA-01-22

Temperature Transients of Fusion-fission Hybrid Reactors in Loss of Coolant Accidents

V. Tang, R. Parker

August 2001

Plasma Science and Fusion Center
Massachusetts Institute of Technology
Cambridge, MA 02139 USA

Temperature Transients of Fusion-fission Hybrid Reactors in Loss of Coolant Accidents

Abstract
In this preliminary scoping study, post-accident temperature transients of several fusion-fission designs utilizing ITER-FEAT-like parameters and fission pebble bed fuel technology are examined using a 1-D cylindrical Matlab heat transfer code along with conventional fission decay heat approximations. Scenarios studied include systems with no additional passive safety features to systems with melting reflectors designed to increase emissivity after reaching a critical temperature. Results show that for fission power densities of 5 to 10 MW/m^3, none of the realistic variants investigated are completely passively safe; the critical time, defined as the time when either any structural part of the fusion-fission tokamak reaches melting point, or when the pebble fuel reaches 1873K, ranges from 5.5 to 80 hours. Additionally, it is illustrated that, fundamentally, the LOCA characteristics of pure fission pebble beds and fusion-fission pebble beds are different. Namely, the former depends on the pebble fuel's large thermal capacity, along with external radiation and natural convective cooling for its passive safety, while the latter depends significantly more on the tokamak's sizeable total internal heat capacity. This difference originates from the fusion-fission reactor's conflicting goal of having to minimize heat transfer to the magnets during normal operation. These results are discussed in the context of overall fusion-fission reactor design and safety.

1. Introduction

Previous studies[1-3] indicate that fusion-fission systems can possess good actinide or breeding capability, depending on design. Because of the possibility of deep sub-critical operation, it is proposed that fusion-fission systems are inherently safer. Ideally, an optimal fusion-fission system should maintain or at least sacrifice very little of fusion's inherent safety, while maximizing the benefits of a driven fission system. However, because of the nature of the system, removal of large decay heat after LOCA will remain a major safety concern.

Therefore, we study complete LOCAs of one possible solution matching safe fission technology with a tokamak—explicitly, the fusion-fission pebble bed[4] reactor. In many ways, the tokamak is readily suited to the pebble bed's low power density and helium coolant, due to its large blanket volume and need of a coolant that is chemically and electro-magnetically inert. In addition, the use of pebble bed fuel might only require slight modification to the tokamak confinement structure; at the very least, a containment building might not be needed. However, these benefits must be weight against the constraints and limitations of a fusion-fission pebble bed system, namely, the restriction to a thermal spectrum and low power densities. For this study, we use the ITER-FEAT reference design for our geometric tokamak parameters.

It can be argued that since the pebble bed fuel form and reactor technology is the safest with respect to LOCAs of fission reactors using solid fuel, an upper bound case for LOC safety of fusion-fission solid fuel systems can be found by analyzing the transients of fusion-fission pebble bed reactor during LOCAs. Scenarios studied for this paper include systems with no additional passive safety features and systems with melting reflectors designed to increase emissivity after reaching a critical temperature. Melting reflectors are passive features that allow greater thermal access to the large heat capacity of the magnets during an accident. Bartels et al. advocate a similar design for ITER[5]. The main variables involved is power density and its distribution in the blanket modules.

Temperature Transients of Fusion-fission Hybrid Reactors in Loss of Coolant Accidents

2. Model and Solution Method

Akin to other scoping studies of potential fusion reactor accidents[5,6], a 1-D cylindrical model was developed. The tokamak is modeled by a series of concentric cylinders. The sections modeled in the reference build are the central solenoid, inner toroidal coils, inner thermal shield, inner vacuum vessel, inner blanket, outer blanket, outer vacuum vessel, outer thermal shield, outer toroidal coils, cryostat thermal shield, and cryostat. The blanket is composed of a rear wall (facing the vacuum vessel), a rear tritium breeding section, a mid-section divider, a fission section made up of graphite spheres, and a first wall. The geometry and material compositions of the 1-D model are based on a mid-plane cut of the ITER-FEAT design. Some of the material volume fractions, such as the vacuum vessel and thermal shields, are estimates; they should be typical of fusion-fission designs utilizing tokamaks similar in size to ITER-FEAT. In order for the volume of the cylindrical model to be comparable to that of ITER-FEAT, the height is set to 10 meters. Additionally, although the blanket structural material considered is SS316, a material the fusion community believes is unattractive for fusion reactor applications, the results are similar even if a different structural material is chosen, since SS316 only makes up several thin sections of the blanket module, along with a small 5% by volume of the breeder section.

An explicit 1-D MATLAB code utilizing nodal cell energy balances was written to solve the coupled radiation, convection, and conduction heat transfer equations. Figure 1 and equations 1-6 illustrates the energy balances and the control volume used by the code.

The governing heat transfer conduction, radiation, and convection equations for the i to i+1 node are[7]:

$$Q_{i,i+1}^{cond}(W) = -\frac{(k_i + k_{i+1})}{2}\frac{T_i - T_{i+1}}{\Delta R}A_{i+0.5} \tag{1}$$

$$Q_{i,i+1}^{rad}(W) = -\frac{\varepsilon_i}{1 + \frac{\varepsilon_i A_{+i}}{\varepsilon_{i+1} A_{i+1}}(1-\varepsilon_{i+1})}\sigma(T_i^4 - T_{i+1}^4)A_{i+0.5} \tag{2}$$

$$Q_{i,i+1}^{conv}(W) = -h_{ci}(T_i - T_{coolant})A_{i+0.5} \tag{3}$$

where k is the thermal conductivity, h_c the convective constant, T the temperature, ε the emissivity, σ the Stefan-Boltzmann constant, ΔR the radial distance between each nodal point, and A, the surface area, given by:

$$A_{i\pm0.5}(m^2) = 2\pi(i\Delta R \pm \frac{\Delta R}{2})\cdot 1m \tag{4}$$

Correspondingly, there are three separate equations for $Q_{i,i-1}$. Summed together, they approximate the total amount of energy into and out of node i at time step t, giving:

$$T_{i,t+1} = \frac{(Q_{i,i+1}^{cond} + Q_{i,i+1}^{rad} + Q_{i,i+1}^{conv} + Q_{i,i-1}^{cond} + Q_{i,i-1}^{rad} + Q_{i,i-1}^{conv} + S_iV_i)\Delta t}{Cp_iV_i} + T_{i,t} \tag{5}$$

where Cp is the specific heat in J/m³ K, S is the source term in J/m³, Δt the time between each time step, and V, the volume, is:

$$V_i(m^3) = \pi((i\Delta R + \frac{\Delta R}{2})^2 - (i\Delta R - \frac{\Delta R}{2})^2)\cdot 1m \tag{6}$$

Similar to the ChemCON[8] studies, the physical model consists of dividing the reactor into components that are connected only by radiation and/or convection, depending on coolant

availability.   Inside each section, heat transfer can occur via radiation, convection and conduction. All thermophysical properties are volume averaged by material and homogenized, with the exception of the thermal conductivity of magnet sections, which is calculated assuming only the volume fraction of steel in the magnet, due to the heavy insulation surrounding the superconductors.

Finally, boundary conditions are also required. For the outer edge (i.e. cryostat), it is assumed that only natural convection and radiation cooling occurs. From previous studies[6], h_c is set at roughly 4W/m^{2}K. The surroundings are assumed to be a black body.

Table 1 provides complete details and a summary of the reference build.

3. Decay Heat Source
In this analysis, the fission blankets (sections 5d and/or 7b) are assumed to be the only source of decay heat.   The decay heats from activated structures and tritium breeding sections are neglected. This assumption is used because in most cases, these other sources of decay heat are very small when compared with the fission fuel source, and are much more design dependent. For preliminary and scoping studies, it should be adequate to account for just the fission product and actinide decay heats

The fission portions of the blanket are assumed to have a uniformed powered density, since the residence time of any fuel pebble is small compared with the irradiation period; otherwise, the blanket would exhibit an exponential decay power density from the front wall.

The main source of decay heat, therefore, follows the conventional U235 fission product approximation[9]:

$$P = 6.6x10^{-2} P_o \left[t^{-0.2} - (t+t_o)^{-0.2} \right] \tag{7}$$

Where P is the decay power, P_o the operating power, t_o the time in seconds that the reactor has been operating at P_o, and t the time after shutdown.

In addition, for a fission reactor fueled with U238, Larmash gives the following for the major actinide decay heat contributions:

$$P_{29} = 2.28x10^{-3} P_o C(\frac{\sigma_{a25}}{\sigma_{f25}}) \left[1 - e^{-4.91x10^{-4} t_o} \right] e^{-4.91x10^{-4} t} \tag{8}$$

$$P_{39} = 2.17x10^{-3} P_o C(\frac{\sigma_{a25}}{\sigma_{f25}}) \left[(1 - e^{-3.41x10^{-6} t_o}) e^{-3.41x10^{-6} t} - 7.0x10^{-3} (1 - e^{-4.91x10^{-4} t_o}) e^{-4.91x10^{-4} t_o} \right] \tag{9}$$

P_{29} and P_{39} are the decay powers of U239 and Np239 respectively. P is the decay power, P_o the operating power, and t_o, assumed to be one year, is the time in seconds that the reactor has been operating at P_o. Finally, C is the conversion factor, assumed to be one (i.e. a converter) in this analysis, and σ_{a25} and σ_{f25} are the effective thermal cross sections of U235. The absorption to fission ratio is assumed to be 1.17.

As expected, the dominant decay heat source is from fission product decays. Figure 2 plots the integrated decay heat from a P_o=1MW/m^3 source vs. time.

Temperature Transients of Fusion-fission Hybrid Reactors in Loss of Coolant Accidents

Correspondingly, there is a similar set of equations for a thermal reactor running on the U233-Th232 cycle. However, for the same amount of power, the decay heat from the U233-Th232 cycle should be comparable.

4. Examined Scenarios and Analysis Criteria

Because of the large number of variables and scenarios possible, choosing a characteristic variable to analyze the decay heat scenarios can be difficult. For this analysis, we chose the key constant t_c, or the critical time. Basically, t_c is the time when either any structural part of the fusion-fission tokamak reaches its melting point, or when the pebble fuel reaches 1873K, since above 1873K significant amounts of fission products can begin to escape. These two criteria are used since main structural failure and/or fission product release constitute irreversible consequences of a major accident, and in theory, are both avoided in the pure fission pebble bed reactor LOCA. For such a passively safe system, t_c is infinite. We have neglected the effects of tritium escape, since, in a fusion-fission system, the largest potential source term is the fission one. Also, it is obvious that structural failure will occur before structural melting, but without a complete stress analysis, a true critical temperature is impossible to determine. The melting point of SS316 is often quoted in a range 1630-1675K; for this analysis we conservatively take 1600K. Considering the nature of our scoping studies, the above criteria, along with temperature vs. time profiles, are adequate for illustrating the LOCA characteristics of the systems examined.

Table 2 summaries the simulations. These scenarios can be divided into three basic sections. Runs A1 look at loading both inner and outer fission blanket sections (5d, 7b) of the reference build with power densities (P_o) from 5 to 10 MW/m^3, in order to determine the transient characteristics of a conventional outboard and inboard fission blanket design. Runs B1 examine the case where fission fuel is loaded only in the outboard fuel blanket (7b), with tritium breeder replacing graphite pebbles in the inboard blanket (i.e. 5d same as 5b). This results in greater total heat capacity with smaller heat thermal conductivity for the inboard blanket. In addition, the decay energy has greater access to the large thermal capacity of the outer vacuum vessel. Mainly, this series is analyzed because many fusion-fission designs in the literature possess fission fuel at the outboard blanket only. The total power from B1 is made equal to A1 in order to directly compare the two configurations. Lastly, Runs A2 and Runs B2 look at the effectiveness of increasing the emissivity of the vacuum vessel and thermal shields from the above configurations to 0.8 after reaching 500K, simulating the melting of reflective coatings designed to prevent heating of the superconductors. From equation 2, we expect a significant improvement in heat transfer between different components of the reactor; for example, raising the emissivities of the vacuum vessel and thermal shields to 0.8 will result in approximately 25 times greater radiation transport between those components.

Crude estimates can be made for the critical time. For low-power density cases, we can assume that heat transport is limited by radiation between the different reactor components; i.e. the internal component diffusion time is short compared with the energy absorption or creation rate. With this criterion, we can use equation 2 to determine which components are radiation bottlenecks. For example, for Run# 1, the first and therefore probable limiting decay heat bottleneck is between the vacuum vessel and thermal shield, since the emissivity coefficient in equation 2 for radiation transport between the vacuum vessel and thermal shield is ~4.5 times

less than the coefficient for transport between the blanket and vacuum vessel. Assuming then that energy transfer is limited only to the blanket and vacuum vessel, we have:

$$\int_0^{t_c} D(t)dt = V_b \int_{T_{ini}}^{1600K} Cp_b(T)dT + V_{vv} \int_{T_{ini}}^{1600K} Cp_{vv}(T)dT \tag{10}$$

where D(t) is the decay heat power, V_b and Cp_b the volume and specific heat of the blanket modules, and V_{vv} and Cp_{vv} the volume and specific heat of the vacuum vessel. Using table 1 and figure 2, this method estimates t_c~55 hours for run #1. Clearly, this method is unemployable when sharp radiation barriers do not exist, or when changing emissivities are involved (e.g. melting reflectors).

For a high-power density case t_c estimate, we make the conservative assumption that due to the rapid decay heat buildup, only very little of the vacuum vessel heat capacity is accessed before the blanket reaches critical temperatures. Thus, we have for t_c:

$$\int_0^{t_c} D(t)dt = V_b \int_{T_{ini}}^{1600K} Cp_b(T)dT \tag{11}$$

where D(t) is again the total decay heat, and V_b and Cp_b the volume and specific heat of the blanket modules. Using table 1 and figure 2, this method estimates t_c~5.7 hours for run #4.

5. Results, Discussion, and Analysis
In this section, we discuss the results of the simulations in detail. Temperature profiles vs. time were calculated for all the runs in table 2. The runs in figures 5-12 are samples chosen for illustration.

5.1 Results
Run Series A1
The results from this series of runs show that an inboard and outboard fission blanket design with fission power densities of 5 to 10W/cc can not achieve complete passive safety, with all cases resulting in melting of the inner blanket first wall. Specifically, t_c and total power follow a power relationship:

$$t_c = 1.14x10^{10}P^{-2.73} \tag{12}$$

where P is total power in MW, and t_c in hours.

Figures 5-6 and 7-8 show that for this series of runs, the decay heat is able to utilize to some extent the vacuum vessel heat capacity. However, the large thermal capacity of the magnets is unused, as evidenced by the low ending temperatures of the toroidal field coils and central solenoid. The lower power density scenarios are better at accessing the heat capacities of different components of the reactor. This is plainly noticed in a comparison of the temperature of the vacuum vessels in figure 5 and figure 7. In the blanket, the low thermal conductivity of the tritium breeder can clearly be seen in the figures, since the maximum temperature difference of the tritium breeder and rear blanket wall is large (~200K for run#4), even though the thickness of the blanket is only 10cm. Lastly, the figures and data reveal that external natural convection and radiation is actually heating the cryostat, since during the entire period, the cryostat thermal shield temperature is lower than the cryostat temperature.

Temperature Transients of Fusion-fission Hybrid Reactors in Loss of Coolant Accidents

The Run# 1 critical time result of 41 hours is relatively close to our rough estimate of 55 hours. Figures 5 and 6 show that the assumptions used for equation 10 are not entirely correct; there is definitely some internal thermal resistance in the blanket, since a difference of >100K exists between the front and rear of the inner blanket walls. Also, neither vacuum vessel in figure 5 or 6 reaches 1600K. Thus, integrating to 1600K in equation 10 proves too generous. Additionally, some heat escapes to the thermal walls protecting the magnets, raising the inner and outer thermal shield temperature to ~1000K and 400K respectively. However, this is not enough to offset the 1600K assumption.

On the other hand, the Run#4 approximate t_c from equation 11 underestimated the simulation slightly; this discrepancy stems from not accounting for the fact that a significant amount of energy is radiated to the vacuum vessel during 6.2 hours. Figures 7 and 8 show that the vacuum vessel reaches ~900K at t_c. On the other hand, this is somewhat balanced by the lower than assumed 1500K to 1300K ending temperatures of the tritium breeder.

Run Series B1
The results show that an outboard only blanket with fission power densities of 7.31 to 14.6W/cc can not achieve complete passive safety, with all cases resulting in melting of the outer blanket first wall. Specifically, t_c and total power follow a power relationship:

$$t_c = 8.19x10^{10} P^{-3.00} \tag{13}$$

where P is total power in MW, and t_c in hours.

Figure 10 shows that for this series of runs, the decay heat is able to utilize the outer vacuum vessel heat capacity. The inner vacuum vessel, and thus all inner sections, is less accessible due to heat trapping in the inner blanket caused by the lower thermal conductivity of Li_2TiO_3. A comparison of the inner section temperatures in figure 5 and 9 show this clearly. The large thermal capacity of the magnets is nearly untapped. As before, the data shows that lower power density scenarios are better at accessing the heat capacities of different components of the reactor. In the blanket, the low thermal conductivity of the tritium breeder can obviously be seen in figures 9; the upper-bound temperature difference of the front Li_2TiO_3 and the rear Li_2TiO_3 sections can be greater than 300K, compared with 50K for the front graphite pebbles and rear tritium breeder sections in figure 5. Lastly, figures 10 and data reveal that, once more, external natural convection and radiation is heating the cryostat.

Run Series A2 and B2
Both of these series are not passively safe, with all cases resulting in melting of the inner and outer blanket first wall, respectively. t_c and total power follow power relationships:

$$t_c = 1.78x10^{12} P^{-3.36} \tag{14}$$

$$t_c = 7.13x10^{11} P^{-3.23} \tag{15}$$

where equation 12 and 13 are for Series A2 and B2 respectively. P is total power in MW, and t_c in hours.

Figures 11 and 12 dramatically show the effect of using melting reflectors. Specifically, the toroidal field coils heat capacities are accessed. Also, in general, the energy is more evenly distributed. A comparison of the vacuum vessel and thermal shielding temperature trends in

figures 11 and 12 after the reflectors have melted, with the trends in A1 (figures 5,6) and B1 (figures 7,8) illustrates this. In addition, figures 11 and 12 demonstrate that when a reflector melts, the component with the melting reflector experiences rapid heating, accompanied with either a sharp drop or rise in temperature of the surrounding component. Lastly, as before, the figures and data reveal that external natural convection and radiation are again heating the cryostat.

5.2 Analysis and Discussion

Several key conclusions are immediately drawn from the critical time and temperature transient data in figures 5-12 and table 2. First, it is clear that none of the configurations are completely passively safe. Second, the use of melting reflectors can have a significant positive effect on t_c. Third, in almost all of the cases, distributing the total fission power onto both inboard and outboard blankets gives a slightly greater t_c than the corresponding outboard only scenario. Fourth, the cryostat temperature data shows that for the power densities considered during time period t_c, external cryostat radiation and cooling has no effect, since all of the decay energy is trapped internally. Finally, equation 10 and 11 are adequate for ballpark figures in low and high density limiting cases.

The fundamental problem is the complex interplay between the heat capacity of the pebbles and the reactor's ability to transfer their decay heat across internal boundaries designed to restrict that very ability during normal operation. Figure 3 and figure 4 are overall pictures of this complex situation. Figure 3 plots the data in table 2 with a "pebble only" case, where no heat transfer occurs. Critical time is marked when the pebbles reach 1600K. This $t_{c\ pebble}$ clearly represents a lower bound for t_c. Figure 4 is a plot of the $t_c / t_{c\ pebble}$ ratios. Specifically, as power density goes up, the critical time for different configurations approaches $t_{c\ pebble}$, based on the premise that decay heat is created so quickly that it is basically trapped in the fission blanket. On the lower power density end, larger sections (i.e. vacuum vessel) of the reactor are accessible for heat storage due to the extended time available from slower decay heat buildup. This results in dramatically higher critical times. Additionally, the figures reveal that there is only a slight difference between the inboard/outboard and outboard fueled only configurations. This implies that the additional heat capacity from replacing the inner graphite spheres with extra tritium breeder and steel is counterbalanced by severely lower thermal conductivity. Lastly, using reflectors that melt can nearly double the critical time for lower power densities, but as stated, the effect lessens with increasing power density.

Concerning equations 10 and 11, it is assumed that the cryostat, and therefore external heating and cooling, plays a very minor (if at all) role in the accident. Realistically, this is a very good assumption. Figures 6,8,10,12 and the data show that heat enters the system during the accident, as evident by the increasing temperature of the cryostat thermal shielding. The rate is very small, approximately 5kW, and is solely due to radiation from the room temperature cryostat. This result illustrates a significant point; fundamentally, the LOCA characteristics of pure fission pebble beds and fusion-fission pebble beds are different. Namely, the former depends on the pebble fuel's large thermal capacity, along with external radiation and natural convective cooling for its passive safety, while the latter depends significantly more on the tokamak's sizeable total internal heat capacity and ability to transfer heat internally only with radiation. This difference originates from the fusion-fission reactor's conflicting goal of having to minimize heat transfer

to the magnets during normal operation; the use of thermal shields and "radiation-transfer only" sections significantly hinders its internal heat transfer capacity. Even with increased internal emissivities (Run series A2 and B2), and therefore, greater access to the enormous heat capacities of the magnets (~2000GJ), none of the scenarios examined benefited from external cooling or radiation before reaching the critical time. This is also in contrast with decay heat scenarios in pure fusion, where much small decay powers create extremely long time constants that permit decay energy to distribute itself internally and allow for external cooling and radiation to have desirable effects.

In summary, the fusion-fission hybrid complete LOCA is dominated by fission decay heat buildup that is rapid compared with the time constants for heat transfer in the reactor.

5.3 Fusion-fission design

For this paper, we concentrated on beyond design-basis accidents; i.e. complete LOCAs without intervention. In reality, because of the inherent necessity of separate cooling loops for different sections of the machine (vacuum vessel, fission blanket, tritium breeding section, magnets, thermal shields, etc), it is inconceivable that some cooling not be activated during an extended accident, especially in a three-day period. Also, in a pebble bed system, it is possible that the operator can remove some of the pebbles easily from the blanket during LOCA.

Concerning the blanket, newer structural materials such as silicon carbide will be immensely beneficial. With a melting point of 2450C and no loss of strength until 1600C, the use of silicon carbide will permit the blanket to tolerate much higher temperatures. In contrast with the first wall melts of the SS316 blankets, the critical events in a silicon carbide blanket fusion-fission reactor will be either vacuum vessel melt or fission product release from above 1873K pebble fuel. Looking at figures 9 and 10, we estimate that the use of SiC in the blanket module could double the critical time to ~160 hours, assuming the vacuum vessel temperature rises to 1600K linearly.

The reflector scheme can be improved by using coatings with different melting temperatures. In the current configuration, the vacuum vessel heat capacity is accessed early, but it can take as long as 40 hours (figure 10) before the toroidal field coils are exploited, since the thermal shields protecting them have to be heated from 80K to 500K. Assuming that the heat capacities of the toroidal coils are available totally, we get t_c~180 hours for run#1 using table 1 and figure 2; this is 3 times the t_c estimate from equation 10. Also, if the emissivities of the magnets can be increased during an accident, the currently untouched solenoid can potentially store significantly more heat.

Aside from the reflector proposal, other more exotic passive schemes could be worth pursuing. Since radiation-only barriers are large restrictions to heat transfer between different components, creating any conduction path between separate components during an accident will be valuable. In a clever design, materials with different rates of thermal expansion might be able to achieve this; during normal operation, the components (e.g. blanket and vacuum vessel) are thermally coupled only by radiation, but in an accident, after reaching certain temperatures, physical contacts would be made passively.

Finally, our results can be viewed as positives for using molten fuel (i.e. FLIBE) in a fusion-fission reactor. In theory, using FLIBE solves the fundamental problem of large decay heat source terms in the reactor, since during normal operation fission products are processed and removed online, and handled by devices in an environment unconstrained by super-conducting magnets and fusion plasmas. In addition, a complete LOCA cannot occur, since the coolant and fuel are intermixed. Overall, compared with pebble beds, much higher power densities could be used safely with FLIBE, if judging only with this paper's criteria.

6. Conclusion

In this preliminary scoping study, post-accident temperature transients of several fusion-fission designs utilizing ITER-FEAT-like parameters and fission pebble bed fuel technology are examined using a 1-D cylindrical Matlab heat transfer code along with conventional fission decay heat approximations. Scenarios studied include systems with no additional passive safety features to systems with melting reflectors designed to increase emissivity after reaching a critical temperature. Results show that for fission power densities of 5 to 10 MW/m^3, none of the realistic variants investigated are completely passively safe; the critical time, defined as the time when either any structural part of the fusion-fission tokamak reaches melting point, or when the pebble fuel reaches 1873K, ranges from 5.5 to 80 hours. The critical time is extended considerably by using melting reflectors, which potentially allows greater and earlier access to the large thermal capacities of the magnets and vacuum vessel. Additionally, it is illustrated that, fundamentally, the LOCA characteristics of pure fission pebble beds and fusion-fission pebble beds are different. Namely, the former depends on the pebble fuel's large thermal capacity, along with external radiation and natural convective cooling for its passive safety, while the latter depends significantly more on the tokamak's sizeable total internal heat capacity. This difference originates from the fusion-fission reactor's conflicting goal of having to minimize heat transfer to the magnets during normal operation. These results are discussed in the context of overall fusion-fission reactor design and safety.

Temperature Transients of Fusion-fission Hybrid Reactors in Loss of Coolant Accidents

References

1. E.Cheng and R.J. Cerbone, Prospect of Nuclear Waste Transmutation and Power Production in Fusion Reactors, TSI Research, Inc., 1995.
2. J.D. Lee and R.W. Moir, Fission-Suppressed Blankets for Fissile Fuel Breeding Fusion Reactors, Journal of fusion Energy, 1 (1981) 299-303.
3. D. Steiner, E. Cheng, R. Miller, D. petti, M. Tillack, L. Waganer et al, The ARIES fusion-neutron source study, UCSD-Eng-0083, 2000.
4. A.C. Kadak, R.G. Ballinger, and J.M. Ryskamp, Advanced Reactor Technology-Modular Pebble Bed Reactor Project, MIT/INEEL First Annual Report, 1999.
5. H.W. Bartels, E. Cheng, M.Gaeta, B. Merrill, and D. Petti, Decay heat removal in the ITER outline design, Fusion Engineering and Design. 31 (1996) 203-219.
6. W.E. Han, Analyses of temperature transients in ITER design concepts following hypothetical loss of cooling accidents, Fusion Engineering and Design. 54 (2001) 413-419.
7. A.F. Mills, Basic heat and Mass Transfer, Irwin, Chicago, 1995.
8. M.J. Gaeta, B.J. Merrill and D.A. Petti, LOCA Temperatures/Hydrogen Generation Study for ITER TAC-4 Design, presented at 11th topical meeting on the Technology of Fusion Energy, New Orleans, USA, June, 1994.
9. J.R. Lamarsh, Introduction to Nuclear Engineering, Addison-Wesley Publishing Co, Reading, 1983.

Temperature Transients of Fusion-fission Hybrid Reactors in Loss of Coolant Accidents

Section No.	Description	Radius (m) & Volume (m^3)	Materials (vol%)	Emissivity	Initial Temp (K)	Heat Capacity (ini. to 1600K, in GJ)
Table 1: Reference Case Radial Build and Details						
1	Central Solenoid	1.3-2.1, 85	Incaloy 908(60%), SC(40%)*	0.05	5	504
2	Inner Toroidal Field Coils	2.2-3.11, 152	SS316(56.7%), SC(5.2%)*, Incaloy(1.8%)	0.05	5	661
3	Inner Thermal Shield	3.11-3.27, 32	SS304(58%)	0.03	80	108
4	Inner Vacuum Vessel	3.27-3.6, 71.2	SS316(40%)	0.214	373.15	170
5	Inner Blanket					195(Total)
5a	Rear Wall	3.62-3.63, 2.3	SS316(100%)	0.2	773.15	9.8
5b	Tritium Breeder Section/Shield	3.63-3.73, 23.1	Li$_2$TiO$_3$ Pellets(58.8%), SS316(5%)	1	773.15	54.2
5c	Wall	3.73-3.74, 2.3	SS316(100%)	1	773.15	10
5d	Fuel Section	3.74-4.07, 81	Pryo Graphite (55%),	1	773.15	110
5e	Front Wall	4.07-4.08, 2.6	SS316(100%)	1	773.15	11
6	Plasma	4.08-8.28, 1631	Void	n/a	n/a	n/a
7	Outer Blanket					433(Total)
7a	Front Wall	8.27-8.28, 5.2	SS316(100%)	1	773.15	22.2
7b	Fuel Section	8.28-8.61, 175	Pryo Graphite(55%)	1	773.15	237
7c	Wall	8.61-8.62, 5.4	SS316(100%)	1	773.15	23.1
7d	Tritium Breeder Section/Shield	8.62-8.71, 49	Li$_2$TiO$_3$ Pellets(58.8%), SS316(5%)	1	773.15	127.5
7e	Rear Wall	8.71-8.72, 5.5	SS316(100%)	0.2	773.15	23
8	Outer Vacuum Vessel	8.74-9.45, 406	SS316(40%)	0.214	373.15	966
9	Outer Thermal Shield	9.45-9.61, 96	SS304(58%)	0.03	80	323
10	Outer Field Coils	9.61-10.60, 200	22% Coils(see sec 2) plus add'n 8.8%SS316	0.05	5	979
11	Cryostat Thermal Shield	13.69-13.75, 52	SS304(50%)	0.03	80	150
12	Cryostat Wall	13.80-13.86, 52	SS304(100%)	0.03 inside, 1 outside	293.15	278

*Superconductor, assumed to be 35% Nb$_3$Sn and 65% Cu

| Table 2: Run Summaries			
Run #	Fission Power Density (MW/m^3)	Net Fission Power (MWt)	Critical Time (hr)
Run Series A1:			
1	5	1242	41
2	6.25	1553	21.3
3	7.5	1864	12.3
4	10	2485	6.2
Run Series B1:			
5	7.3	1242	43.5
6	9.14	1553	21.8
7	10.97	1864	11.7
8	14.62	2485	5.5
Run Series A2:			
9	5	1242	79.5
10	6.25	1553	33
11	7.5	1864	18.6
12	10	2485	8.3
Run Series B2:			
13	7.3	1242	75
14	9.14	1553	31.3
15	10.97	1864	18.3
16	14.6	2485	7.1

Temperature Transients of Fusion-fission Hybrid Reactors in Loss of Coolant Accidents

Figure Captions:

Figure 1: Illustration of 1-D cylindrical grid. Q can be from conduction, radiation, or convection.

Figure 2: Integrated decay heat from a 1MW/m^3 operating power U235-238 fission source.

Figure 3: Critical time vs. total power.

Figure 4: Critical time ratio vs. total power.

Figure 5: Maximum temperature vs. time for run#1 inner components. From top to bottom: pebble fuel(dashdot), tritium breeder(dot), blanket rear wall(solid), vacuum vessel (dash), thermal shield (dashdot), toroidal coils(dot), central solenoid(solid). The inner first wall and blanket divider wall are not plotted since they follow the pebble fuel and tritium breeder curves almost exactly.

Figure 6: Maximum temperature vs. time for run#1 outer components. From top to bottom (right hand-side): pebble fuel(solid), tritium breeder(dot), blanket rear wall(dotdash), vacuum vessel(dash), thermal shield(dot), cryostat (solid), cryostat thermal shield(dashdot), toroidal coils(dot).   The outer first wall and blanket divider wall are not plotted since they follow the pebble fuel and tritium breeder curves almost exactly.

Figure 7: Maximum temperature vs. time for run#4 inner components. From top to bottom: pebble fuel(dashdot), tritium breeder(dot), blanket rear wall(solid), vacuum vessel (dash), thermal shield (dashdot), central solenoid(solid). The inner first wall and blanket divider wall are not plotted since they follow the pebble fuel and tritium breeder curves almost exactly. In addition, the toroidal coil curve matches the central solenoid.

Figure 8: Maximum temperature vs. time for run#4 outer components. From top to bottom (right hand-side): pebble fuel(solid), tritium breeder(dot), blanket rear wall(dotdash), vacuum vessel(dash), cryostat (solid), cryostat thermal shield(dashdot), thermal shield(dot), toroidal coils(dot).   The outer first wall and blanket divider wall are not plotted since they follow the pebble fuel and tritium breeder curves almost exactly. In addition, thermal shield and cryostat thermal shield are nearly covered by each other.

Figure 9: Maximum temperature vs. time for run#5 inner components. From top to bottom: front tritium breeder(dashdot), back tritium breeder(dot), blanket rear wall(solid), vacuum vessel (dash), thermal shield (dashdot), toroidal coils(dot), central solenoid(solid). The inner first wall and blanket divider wall are not plotted since they follow the pebble fuel and tritium breeder curves almost exactly.

Figure 10: Maximum temperature vs. time for run#5 outer components. From top to bottom (right hand-side): pebble fuel(solid), tritium breeder(dot), blanket rear wall(dotdash), vacuum vessel(dash), thermal shield(dot), cryostat (solid), cryostat thermal shield(dashdot), toroidal coils(dot).   The outer first wall and blanket divider wall are not plotted since they follow the pebble fuel and tritium breeder curves almost exactly.

Figure 11: Maximum temperature vs. time for run#9 inner components. From top to bottom: pebble fuel(dashdot), tritium breeder(dot), blanket rear wall(solid), vacuum vessel (dash), thermal shield (dashdot), toroidal coils(dot), central solenoid(solid). The inner first wall and blanket divider wall are not plotted since they follow the pebble fuel and tritium breeder curves almost exactly.

Figure 12: Maximum temperature vs. time for run#9 outer components. From top to bottom (right hand-side): pebble fuel(solid), tritium breeder(dot), blanket rear wall(dotdash), vacuum vessel(dash), thermal shield(dot), toroidal coils(dot), cryostat (solid), cryostat thermal shield(dashdot).   The outer first wall and blanket divider wall are not plotted since they follow the pebble fuel and tritium breeder curves almost exactly.

Figure # 1

$$Q_{i,i-1} \longrightarrow \longleftarrow Q_{i,i+1}$$

$$\Delta R$$

i-1   i   i+1
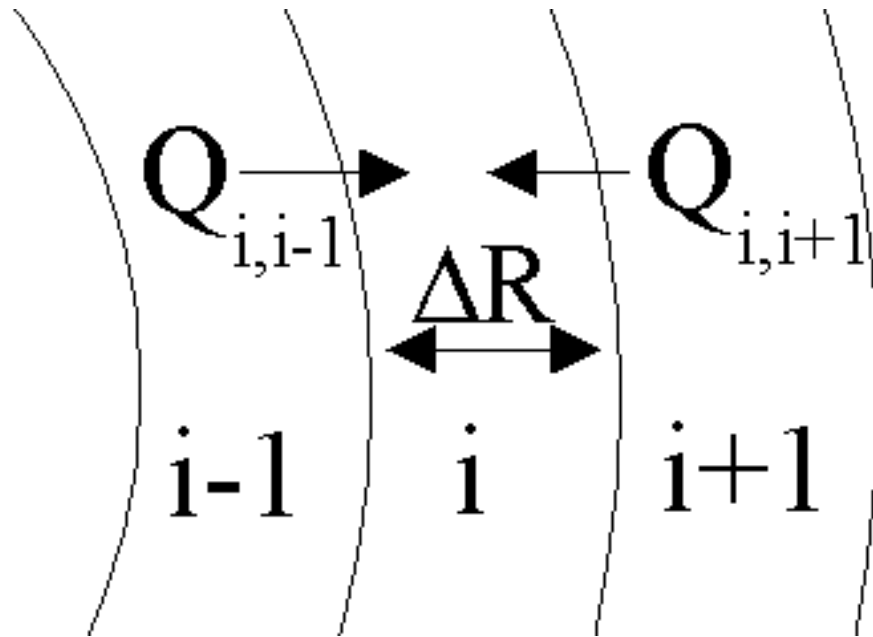
Temperature Transients of Fusion-fission Hybrid Reactors in Loss of Coolant Accidents
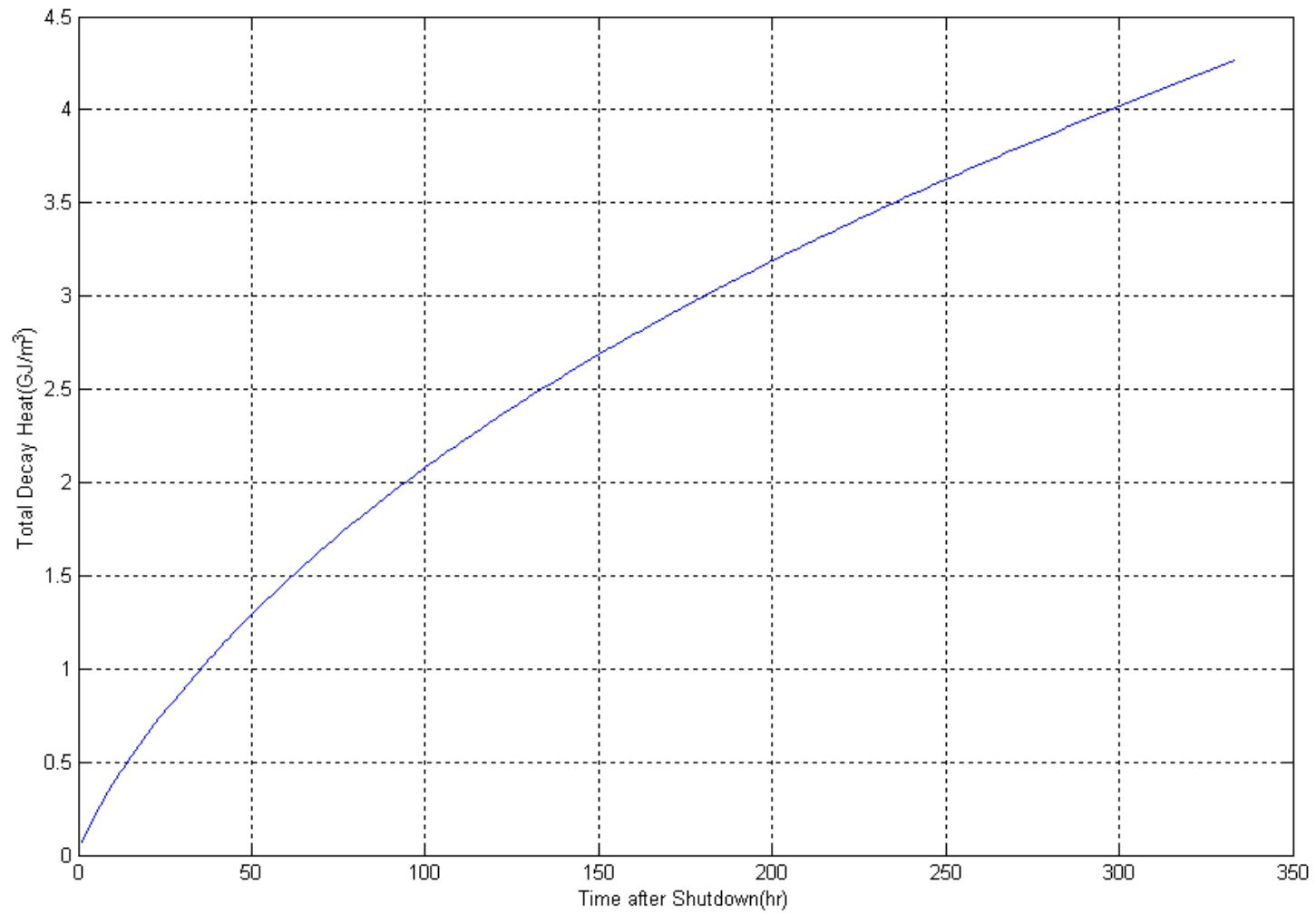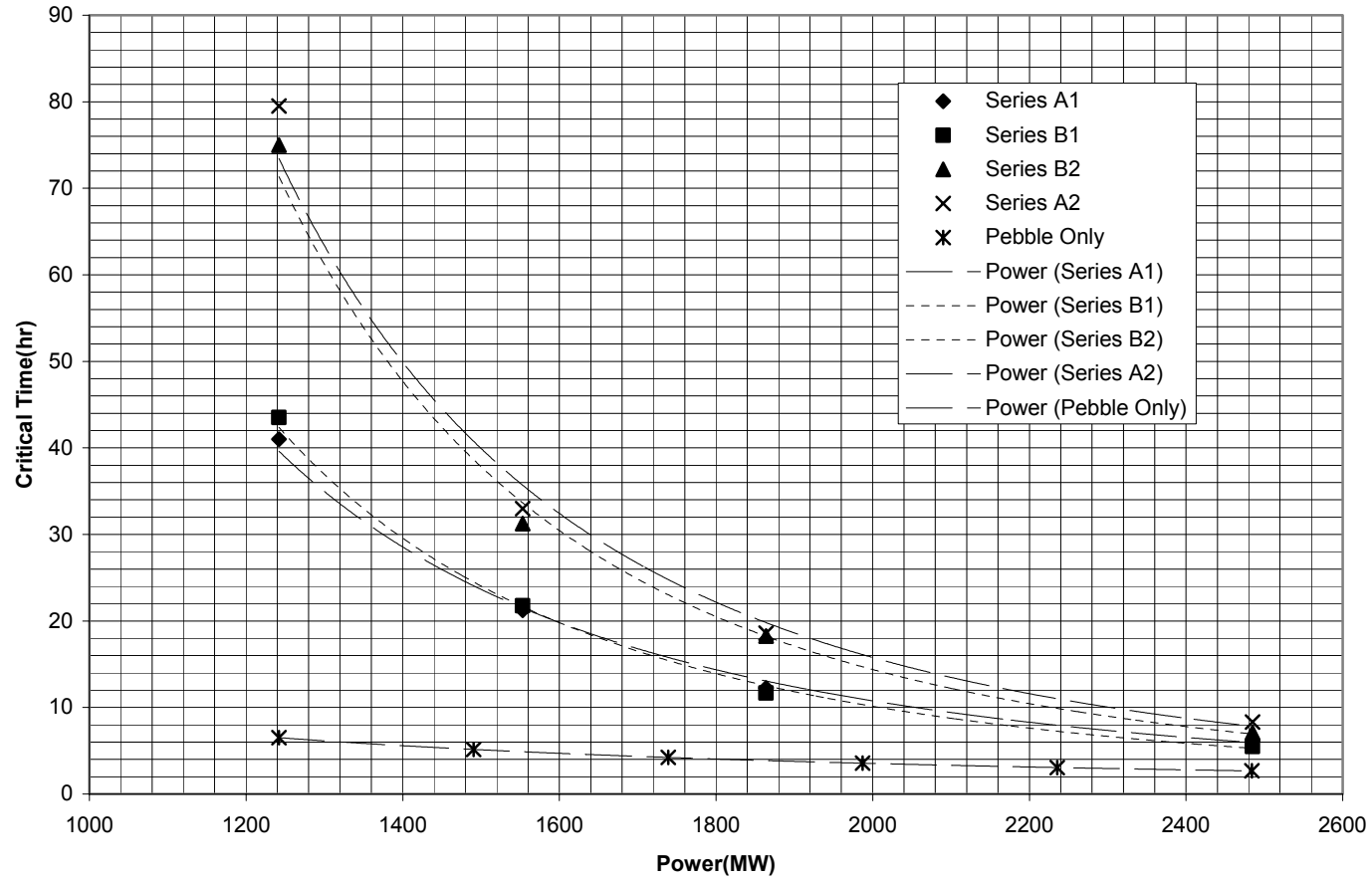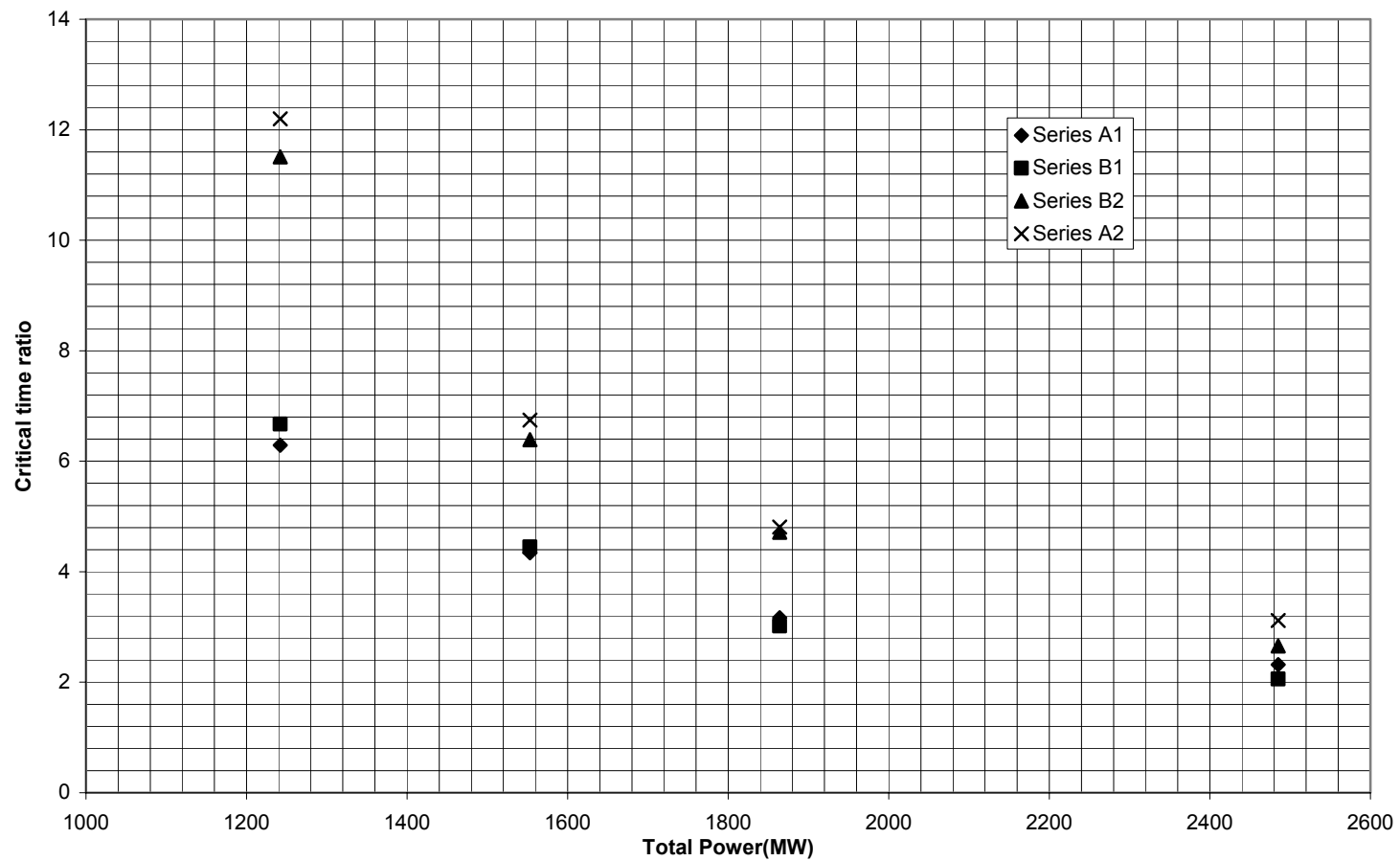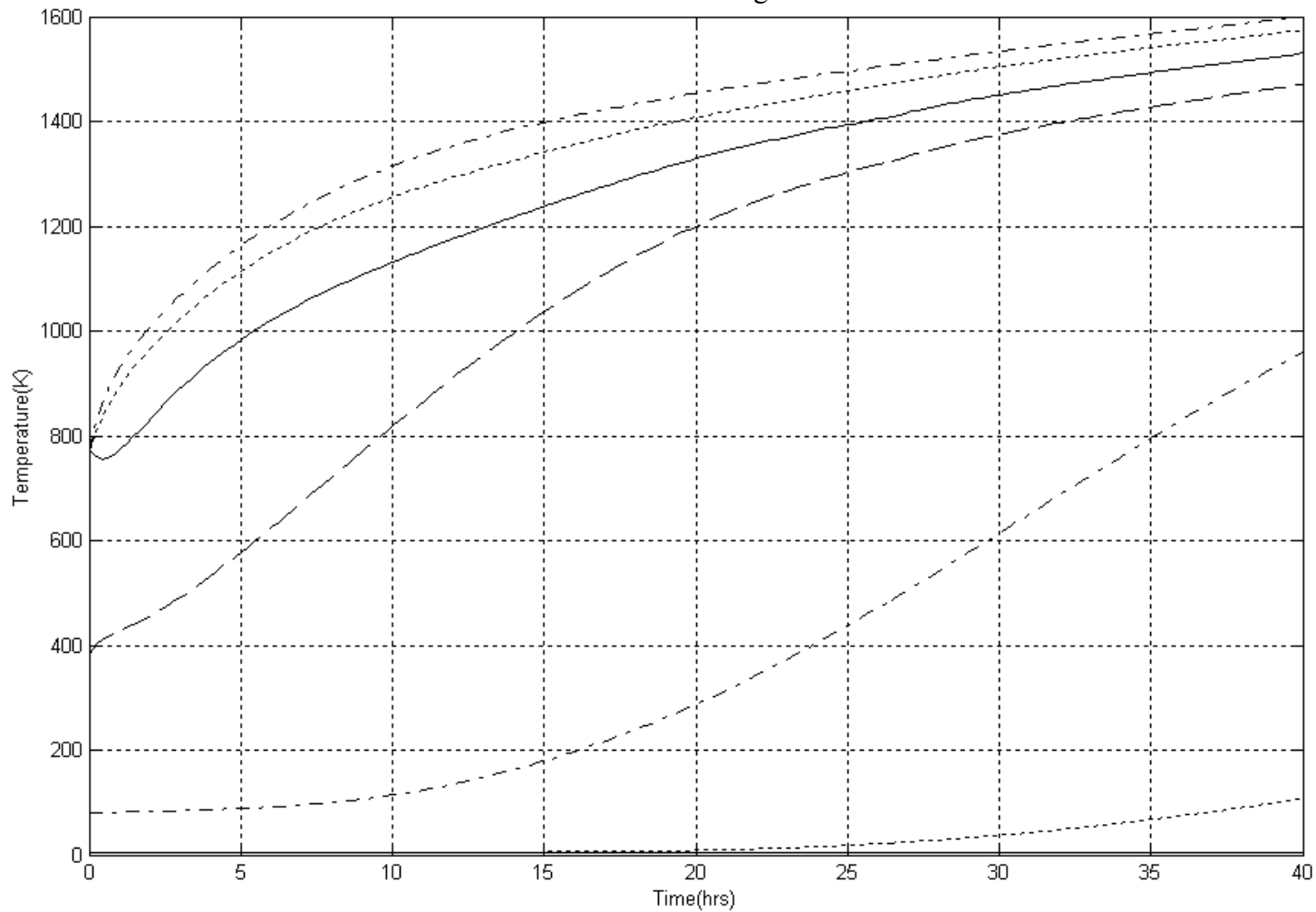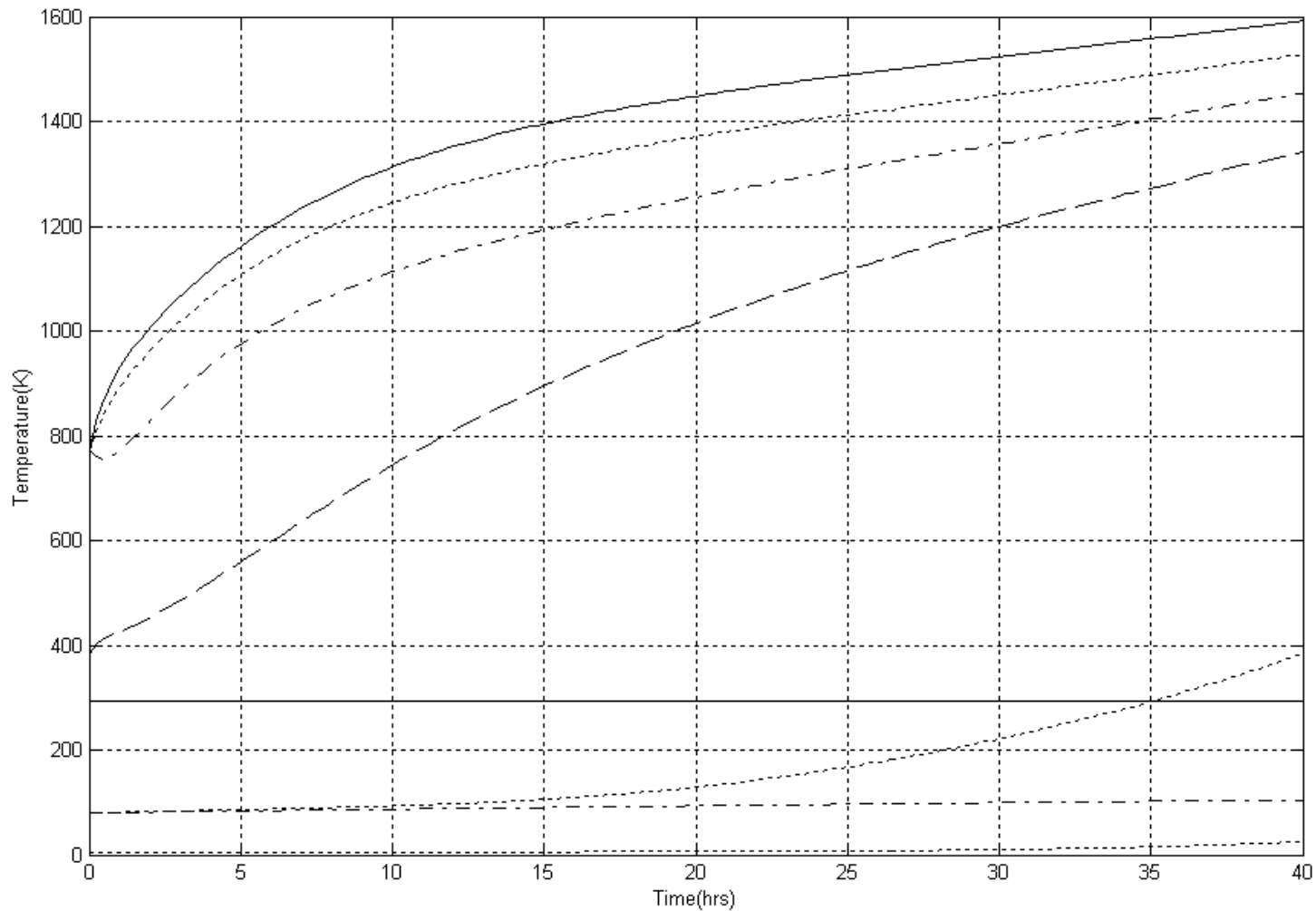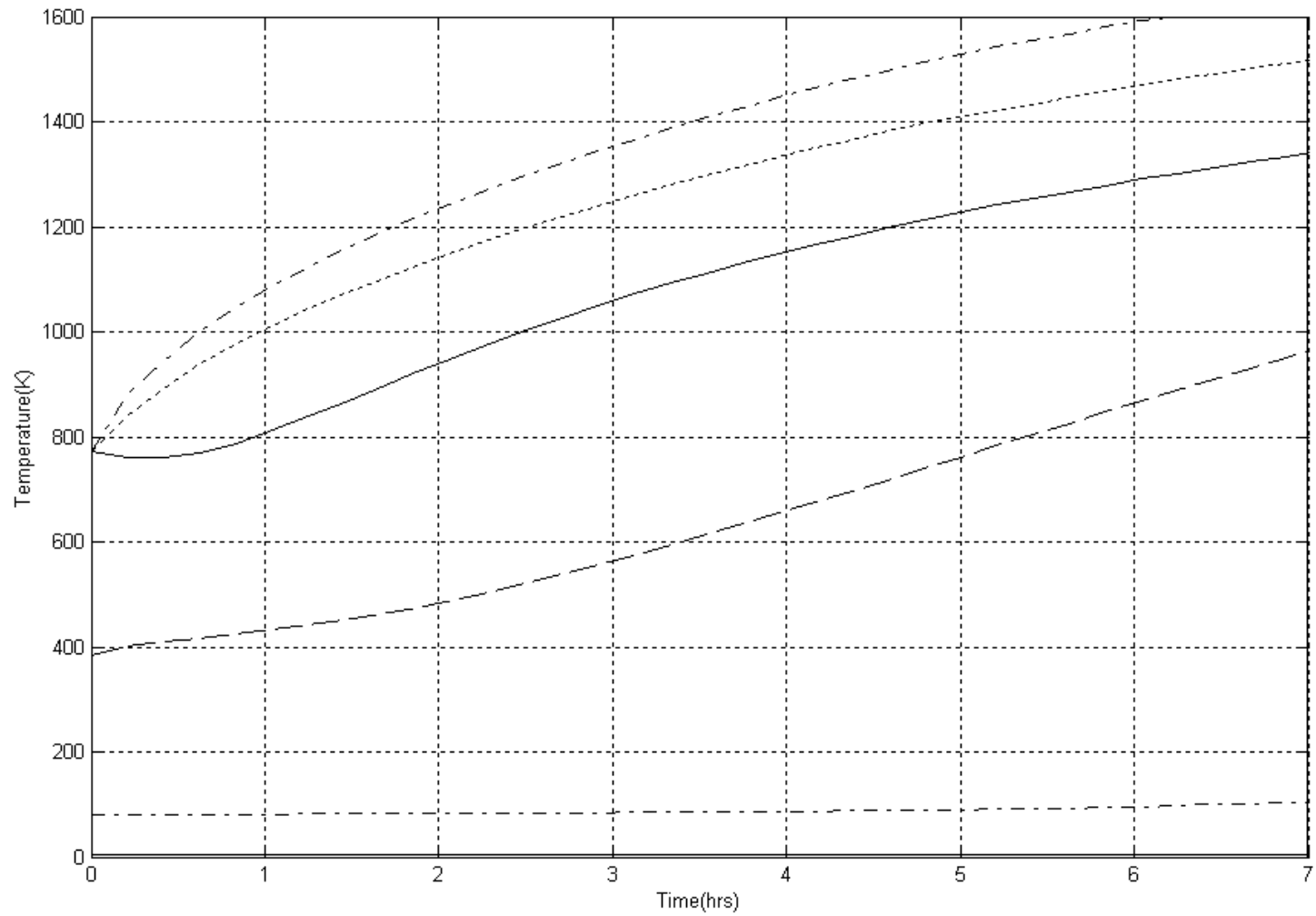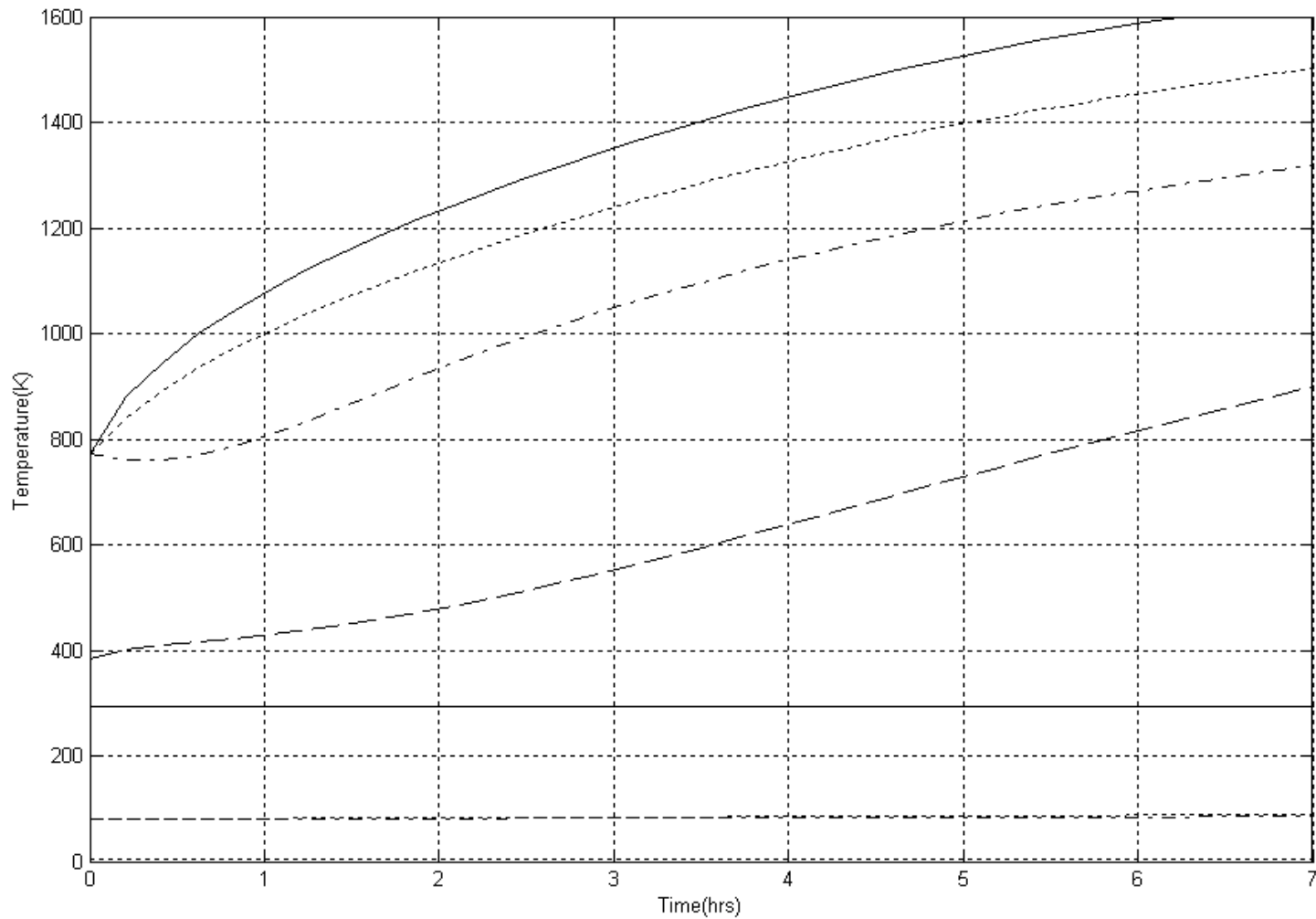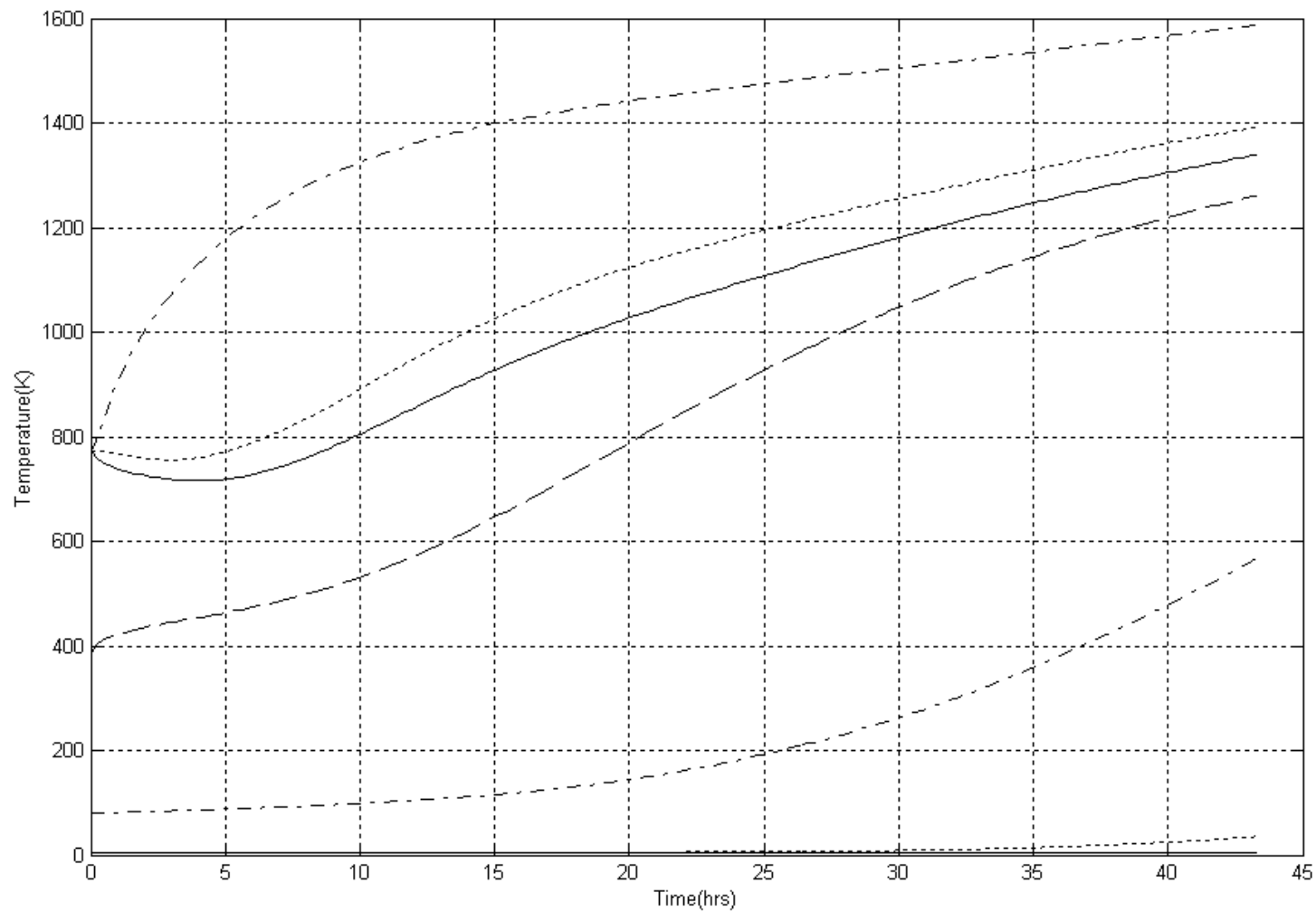
Figure # 2

Figure # 3

Figure # 4

Temperature Transients of Fusion-fission Hybrid Reactors in Loss of Coolant Accidents

Figure # 5

Temperature Transients of Fusion-fission Hybrid Reactors in Loss of Coolant Accidents
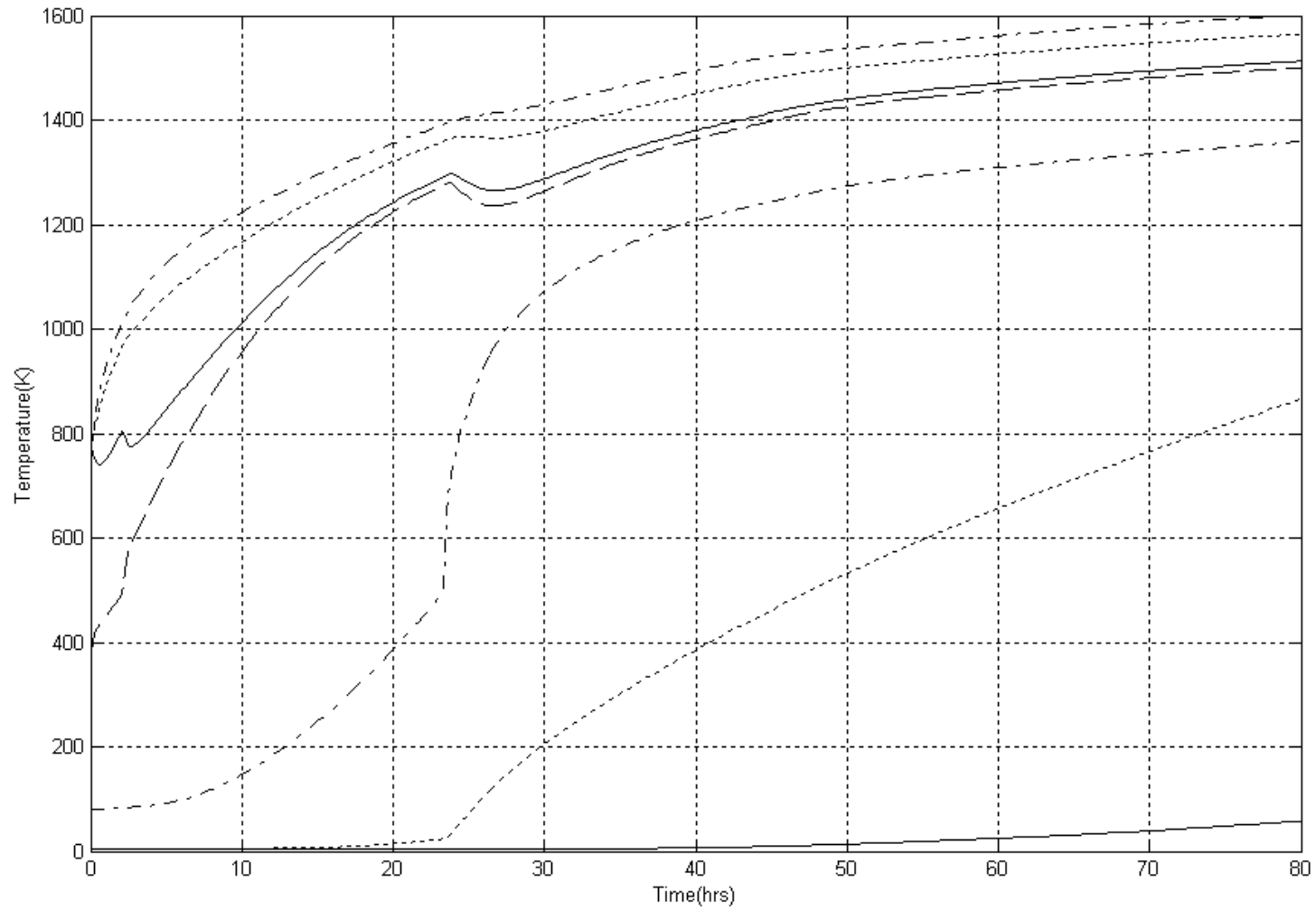
Figure # 6

Temperature Transients of Fusion-fission Hybrid Reactors in Loss of Coolant Accidents

Figure # 7

Temperature Transients of Fusion-fission Hybrid Reactors in Loss of Coolant Accidents

Figure # 8

Temperature Transients of Fusion-fission Hybrid Reactors in Loss of Coolant Accidents

Figure # 9

Figure # 10

Temperature Transients of Fusion-fission Hybrid Reactors in Loss of Coolant Accidents

Figure # 11

Temperature Transients of Fusion-fission Hybrid Reactors in Loss of Coolant Accidents

Figure # 12